P. SARKANYCH,[1,2] YU. HOLOVATCH,[2] R. KENNA [3]

[1] Department for Theoretical Physics, Ivan Franko National University of Lviv
(12 Drahomanov St., 79005 Lviv, Ukraine)
[2] Institute for Condensed Matter Physics of the National Academy of Sciences of Ukraine
(79011 Lviv, Ukraine; e-mail: petrosark@gmail.com)
[3] Applied Mathematics Research Centre, Coventry University
(Coventry CV1 5FB, UK)

PACS 64.60.De, 75.40.Cx

ON THE PHASE DIAGRAM OF THE 2d ISING MODEL WITH FRUSTRATING DIPOLE INTERACTION

Due to intrinsic frustrations of interaction, the 2d Ising model with competing ferromagnetic short-range nearest-neighbour and antiferromagnetic long-range dipole interactions possesses a rich phase diagram. The order of the phase transition from the striped $h = 1$ phase to the tetragonal phase that is observed in this model has been a subject of recent controversy. We address this question by using the partition function density analysis in the complex temperature plane. Our results support the second-order phase transition scenario. To measure the strength of the phase transition, we calculate the values of specific heat critical exponent α. Along with the space dimension, it appears to depend on the ratio of strengths of the short-range and long-range interactions.

Keywords: frustrations, phase transition, density of partition function zeros, critical exponents.

1. Introduction

Pattern formation is one of the fascinating phenomena that may be induced by competing long- and short-range interactions in many-particle physical systems. To give a few examples, a competition of a short-range interaction and the long-range dipole one leads to a variety of experimentally observed structures in ultrathin magnetic films on metal substrates, liquid crystals, polymer films, two-dimensional electron gases, Langmuir and lipid monolayers, etc. (see [1] for more detailed references). Being a subject of intensive experimental studies revealing unusual physical effects, the above systems have important industrial applications. In particular, the aforementioned ultrathin magnetic films became a subject of especial interest due to their possible application in creating high-density storage devices [2].

Theoretical insight into peculiarities of the pattern formation in the above systems has been gained by analysing the 2d Ising model with competing ferromagnetic short-range nearest-neighbour interactions (with strength given by J) and antiferromagnetic long-range dipole interactions (of strength g) [1, 3–12]. In the framework of this model, the richness of the phase diagram is attributed to frustrations introduced by the competing character of ferromagnetic and antiferromagnetic interactions. Analytical approaches, supported by numerical simulations, show that, depending on the values of J and g, the low-temperature phase of this model is characterized by spin configurations classified as regular and irregular checkerboards or stripes of different widths h [1] with spins oriented in a similar direction [3–7]. Evidence of modulated phases has been reported for the J/g ratio near the boundary between striped phases of widths h and $h + 1$ [11]. The above low-temperature magnetic patterns have much in common with those observed in liquid crystals, and the striped, modulated, and paramagnetic phases are often referred to as smectic, nematic, and tetragonal ones. In the latter case, the strip domains are mutually perpendicular. Moreover, already the mean field analysis reveals that the domain-wall structure in such films is similar to 2d liquid crystals [8].

The papers cited above agree in general on the classification of patterns observed in the 2d Ising model with competing nearest-neighbour and dipole interactions. However, the detailed form of the phase dia-

[1] Here and below, h is the stripe width measured in lattice units.

gram remains still unclear. In particular, a subject of the recent discussion has been the form of the phase diagram in the region of low values of temperature T and $\delta = J/g$ (a sketch of the phase diagram in this region is shown in Fig. 1). Whereas the temperature-induced phase transitions from the antiferromagnetic checkerboard-like phase (AF) and from the striped $h = 2$ phase to the tetragonal phase are of the second and of the first order, respectively, the order of the phase transition between the striped $h = 1$ phase and the tetragonal phase is the subject of the discussion. In particular, the MC simulations of Ref. [11] manifest a second-order phase transition in the region $\delta < 0.8$ and the first-order transition in the region $0.83 < \delta < 0.88$. As a consequence, a tricritical point has been predicted in between the two regions. The subsequent MC simulations of Ref. [12] did not observe the conjectured tricritical point and resulted in a continuous phase transition for all region of δ that corresponds to the boundary between the striped $h = 1$ and tetragonal phases (see Fig. 1). The simulations were supported by the analysis of the partition function zeros in the complex temperature plane (Fisher zeros) [13].

In our study, we will complement the analysis of the phase diagram of the 2d Ising model with competing nearest-neighbour and dipole interactions by considering the density of partition function zeros [14]. In particular, this will allow us to avoid a hyperscaling assumption, while calculating the strength of the phase transition, and to directly obtain the specific heat critical exponent α. The input data for our analysis are provided by the coordinates of the partition function zeros calculated in [12]. The rest of the paper is organized as follows: in Sections 2 and 3, we describe the model and the method used for its analysis. Our results are presented and discussed in Section 4.

2. Ising Model with Dipole Interaction

The Hamiltonian of the 2d Ising model with competing ferromagnetic nearest-neighbour and antiferromagnetic dipole interactions reads

$$H = -\delta \sum_{<i,j>} \sigma_i \sigma_j + \sum_{i<j} \frac{\sigma_i \sigma_j}{r_{ij}^3}. \qquad (1)$$

Here, $\delta = J/g > 0$, J and g being the strengths of the nearest neighbour and dipole interactions, respectively. The summation is performed over the sites of the $L \times L$ square lattice. The first sum in (1) spans all pairs of nearest-neighbour Ising spins $\sigma_i = \pm 1$, while all pairs of lattice sites are taken into account in the second term. The Ising spins are supposed to be aligned out of the plane.

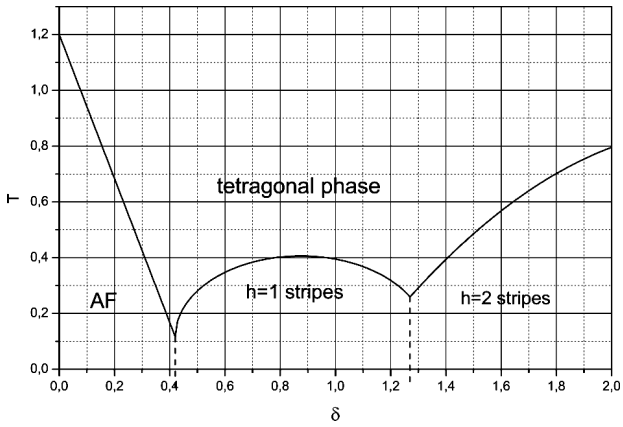

Fig. 1. Phase diagram of the 2d Ising model with competing nearest neighbour and dipole interactions (sketched from Refs. [11,12]). AF: checkerboard antiferromagnet phase, $h = 1$, $h = 2$: striped phases

In the limiting cases of $J = 0$ or $g = 0$ (i.e. δ equals 0 or ∞), Hamiltonian (1) presents a pure dipole interaction model or the usual Ising model, respectively. Both cases are characterized by a single (antiferro- or ferromagnetic) low-temperature phase and by a continuous second-order phase transition to the paramagnetic state. Note that the aforementioned antiferromagnetic-to-paramagnetic phase transition belongs to the universality class of the 2d Ising model too [10, 15]. The phase behaviour of model (1) is much more complicated for nonzero δ, as was briefly described in Introduction. The part of the phase diagram of the model in the region of small δ of the $T - \delta$ plane is sketched in Fig. 1.

The previous analyses of the phase diagram were performed either by numerical or analytical tools, based on the calculation of the partition function

$$Z_L(\beta) = \mathrm{Tr} \exp(-\beta H), \qquad (2)$$

where $\beta = 1/T$, and the trace is performed over all spin configurations. The analysis we report upon in this paper relies on the examination of the partition function behaviour in the complex T (complex β) plane. Since the pioneering papers of Lee and Yang

[16] and Fisher [13], where the partition function zeros in the complex field and complex temperature planes were studied, this type of analysis became a powerful tool to study phase transitions in various models. For the model under consideration (1), it has been recently applied in Ref. [12], where the first zero of the partition function closest to the origin has been calculated for different values of interaction ratio δ at different lattice sizes $L = 12$–72. The finite-size scaling (FSS) analysis of zeros' coordinates allows one to obtain the value of correlation length critical exponent ν. The value of $d\nu$ is given in the Table for different values of δ. Provided that the hyperscaling relation $\alpha = 2 - d\nu$ holds, one can use it to obtain the specific heat critical exponent α. Corresponding $\alpha(\delta)$ values are quoted in the third column of the Table. Since $\alpha = 1$ for the first-order phase transitions, the obtained values of the exponents $\alpha < 1$ serve an evidence of a second-order phase transition in the considered region of δ. This result has been further supported by a FSS analysis of the specific heat, leading to the ratio α/ν that is quoted in the fourth column of the Table [12]. Again, using the hyperscaling relation, one can extract the value of α at $d = 2$ via $\alpha = \frac{2\alpha/\nu}{d+\alpha/\nu}$. The last value is shown as a function of δ in the fifth column of the Table. The sixth column contains our results obtained via the partition function zeros density analysis ($\alpha_{\rm zd}$).

We note that, although the above-obtained estimates for α support a continuous phase-transition scenario ($\alpha < 1$), they do not agree numerically. Moreover, the methods used for their determination do not deliver their direct evaluation, but rather rely on hyperscaling relations. Therefore, in the forthcoming section, we will use the alternative partition-function-zeros analysis that allows the direct determination of the exponent α.

Critical exponents of the 2d Ising model with competing ferromagnetic nearest-neighbour and antiferromagnetic dipole interactions for different values of the interaction ratio δ

δ	$d\nu$ [12]	$\alpha = 2 - d\nu$	α/ν [12]	$\alpha = \frac{2\alpha/\nu}{d+\alpha/\nu}$	α_{zd}
0.89	1.807(70)	0.193(70)	0.364(20)	0.308(17)	0.194(17)
0.91	1.817(68)	0.183(68)	0.375(19)	0.316(16)	0.191(14)
0.93	1.779(61)	0.221(61)	0.399(20)	0.333(17)	0.221(16)
0.95	1.741(53)	0.259(53)	0.424(20)	0.350(17)	0.255(14)
0.97	1.706(46)	0.294(46)	0.461(19)	0.375(16)	0.292(14)
1.00	1.659(37)	0.341(37)	0.522(17)	0.414(14)	0.349(13)
1.10	1.415(25)	0.585(25)	0.888(21)	0.615(15)	0.5882(84)
1.20	1.223(21)	0.777(21)	1.496(28)	0.856(16)	0.788(17)
1.30	1.0093(28)	0.9907(28)	2.0183(66)	1.0046(33)	1.011(13)

3. Density of Partition Function Zeros

In our analysis, we will use the method of analysing the density of partition function zeros originally suggested in [14]. A particular advantage of this method is that it allows one to discriminate between the first- and second-order (as well as higher order) phase transitions and to measure the strengths of first- and second-order phase transitions in the form of the latent heat and critical exponents. Below, we briefly describe the main steps of the partition function zeros density analysis. Provided that the zeros of the partition function of the model (given by (2) in our particular case) in the complex plane are known, one can write it in the factorized form

$$Z_L(z) = A(z) \prod_j (z - z_j(L)), \tag{3}$$

where z stands generically for an appropriate function of the complex temperature (in the Fisher case) or complex field (in the Lee–Yang case), L is the linear extent of the lattice, and $A(z)$ is a smooth function that never vanishes. The free energy density follows as

$$f_L(z) = \frac{1}{L^d} \ln Z_L(z) =$$

$$= \frac{1}{L^d} \left(\ln A(z) + \sum_j \ln (z - z_j(L)) \right). \tag{4}$$

The first term on the right contributes only to the regular part of thermodynamic functions and will be dropped henceforth. The remainder, which will be referred to as $f_L^{\rm s}(z)$, gives rise to a singular behavior.

It is suitable to parametrize the zeros by

$$z = z_c + r \exp(i\varphi), \tag{5}$$

where z_c is a critical point coordinate. Let us define the density of zeros as

$$g_L(r) = L^{-d} \sum_j \delta(r - r_j(L)), \tag{6}$$

with $z_j = z_c + r_j \exp(i\varphi)$. Subsequently, the free energy and the cumulative distribution function of zeros are defined as

$$f_L^{\rm s}(z) = \int_0^R g_L(r) \ln(z - z_c - re^{i\varphi}) dr + \text{c.c.}, \tag{7}$$

$$G_L(r) = \int_0^r g_L(s) ds = \begin{cases} = \dfrac{j}{L^d}, \text{ if } r \in (r_j, r_{j+1}), \\ = \dfrac{2j-1}{2L^d}, \text{ if } r = r_j, \end{cases} \tag{8}$$

where c.c. means complex conjugate, and R is some appropriate cutoff. In the thermodynamic limit and for first-order phase transitions, Lee and Yang already have shown [16] that the density of zeros has to be non–zero crossing the real axis. This corresponds to the cumulative distribution of zeros

$$G_\infty(r) = g_\infty(0) r + b r^{w+1} + ..., \tag{9}$$

where the slope at the origin is related to the latent heat (or magnetization) via

$$\Delta e \propto g_\infty(0). \tag{10}$$

Furthermore, it has been shown (see [17, 18]) that the necessary and sufficient condition for the specific heat at second-order phase transitions to have the leading critical behaviour $C \sim t^{-\alpha}$, is

$$G_\infty(r) \propto r^{2-\alpha}. \tag{11}$$

The above survey leads to the conclusions that a plot of $G_L(r_j) = (2j-1)/2L^d$ against $r_j(L)$ should: (i) go through the origin, (ii) display L- and j-collapse, and (iii) reveal the order and the strength of a phase transition by its slope near the origin. In the next section, we will give results of an analysis of corresponding plots for the partition function (2) of the model with Hamiltonian (1).

4. Results and Conclusions

As has been stated in Introduction, the input data for our analysis are provided by the coordinates of the partition function zeros calculated in [12] for different δ and L. From these, we calculate $G(r)$ dependence of the cumulative density function (8) for various values of δ. Obtained in this way, a typical $G(r)$ plot is shown in Fig. 2 for $\delta = 1$. Subsequently, the set

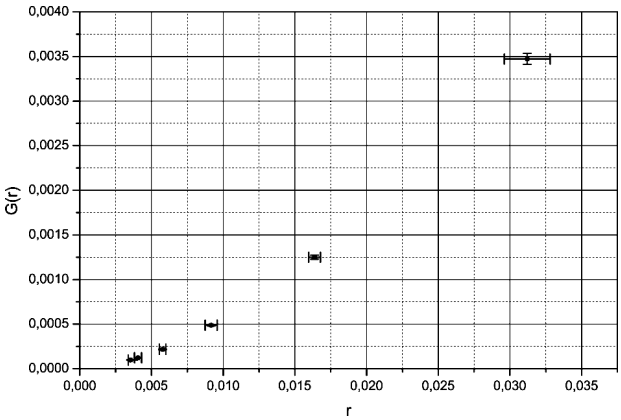

Fig. 2. Cumulative density function $G(r)$ for $\delta = 1$

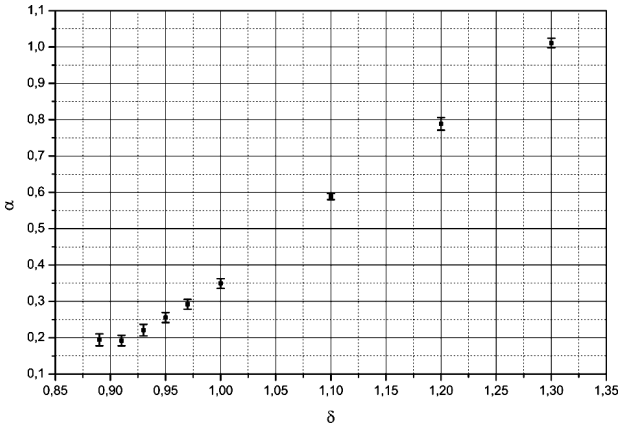

Fig. 3. Dependence of the critical exponent α calculated in this study ($\alpha_{\rm zd}$) on the interaction parameter δ

of functions $G(r)$, for every value of δ, is fitted with $G(r) = ar^{2-\alpha} + b$. The resulting values of the specific heat critical exponent α_{zd} are listed in the last column of the Table.

There are several conclusions one can make comparing the data for the specific heat exponents from the Table. First of all, it is worth noting that the results obtained by three different techniques: (i) FSS of partition function zeros (third column of the Table, obtained by a hyperscaling relation from data of Ref. [12]), (ii) FSS of the specific heat [12] (fifth column of the Table) and (iii) density of partition function zeros analysis (last column of the Table, our data) give value of $\alpha < 1$ up to $\delta < 1.3$. Recalling that that $\alpha = 1$ serves as the evidence for a first-order phase transition (cf. Eqs. (7) and (9)), one can conclude that the transition from the striped $h = 1$ to

the tetragonal phase (see the phase diagram in Fig. 1) occurs through a continuous transition scenario. For the values of $\delta \geq 1.3$ all three approaches predict a first-order phase transition, leading to the conclusion that the tricritical point is located in the region $1.2 < \delta < 1.3$.

All three approaches deliver the δ-dependent values of critical exponents, making δ along with the space dimension d the global variable that defines the universality class. The dependence of the critical exponent α calculated in this study ($\alpha_{\rm zd}$) on the interaction parameter δ is shown in Fig. 3. Let us note, however, that the numerical values of exponents obtained via different approaches differ. In particular, the results of the FSS analysis of partition function zeros (third column of the Table) are in good agreement with the analysis of the density of partition function zeros (sixth column of the Table). But they essentially differ from the results obtained on the basis of the FSS analysis of the specific heat behaviour [12]. This result calls for a further investigation.

This work is supported in part by FP7 Marie Curie Action grants PIRSES-GA-2011-295302-SPIDER and PIRSES-GA-2010-269139-DCP-PhysBio. P.S. acknowledges the useful discussion during the conference of young scientists at the Bogolyubov Institute for Theoretical Physics (Kyiv, Ukraine, December 24–27, 2013), where this work was presented.

1. A. Giuliani, J.L. Lebowitz, and E.H. Lieb, Phys. Rev. B **74**, 064420 (2006).
2. D. Pescia and V.L. Pokrovsky, Phys. Rev. Lett. **65**, 2599 (1990).
3. A.B. MacIsaac, J.P. Whitehead, M.C. Robinson, and K. De'Bell, Phys. Rev. B **51**, 16033 (1995).
4. Ar. Abanov, V. Kalatsky, V.L. Pokrovsky, and W.M. Saslow, Phys. Rev. B **51**, 1023 (1995).
5. I. Booth, A.B. MacIsaac, J.P. Whitehead, and K. De'Bell, Phys. Rev. Lett. **75**, 950 (1995).
6. A. Vaterlaus *et al.*, Phys. Rev. Lett. **84**, 2247 (2000).
7. S.A. Cannas, D.A. Stariolo, and F.A. Tamarit, Phys. Rev. B **69**, 092409 (2004).
8. A.B. Kashuba and V.L. Pokrovsky, Phys. Rev. B **48**, 10335 (1993).
9. P.M. Gleiser, F.A. Tamarit, and S.A. Cannas, Physica D **73**, 168 (2002).
10. E. Rastelli, S. Regina, and A. Tassi, Phys. Rev. B **73**, 144418 (2006).
11. E. Rastelli, S. Regina, and A. Tassi, Phys. Rev. B **76**, 054438 (2007).
12. J.S.M. Fonseca, L.G. Rizzi, and N.A. Alves, Phys. Rev. E **86**, 011103 (2012).
13. M.E. Fisher, in: Lecture in Theoretical Physics, Vol. VIIC, ed. W.E. Brittin (Gordon and Breach, New York, 1968); p. 1.
14. W. Janke and R. Kenna, J. Stat. Phys. **102**, 1211 (2001).
15. A.B. MacIsaac, J.P. Whitehead, K. De'Bell, and K.S. Narayanan, Phys. Rev. B **46**, 6387 (1992).
16. C.N. Yang and T.D. Lee, Phys. Rev. **87**, 404 (1952).
17. R. Abe, Prog. Theor. Phys. **37**, 1070 (1967); Prog. Theor. Phys. **38**, 72 (1967); Prog. Theor. Phys. **38**, 322 (1967); Prog. Theor. Phys. **38**, 568 (1967).
18. M. Suzuki, Prog. Theor. Phys. **38**, 289 (1967); Prog. Theor. Phys. **38**, 1225 (1967); Prog. Theor. Phys. **38**, 1243 (1967); Prog. Theor. Phys. **39**, 349 (1968).
19. C. Itzykson, R.B. Pearson, and J.B. Zuber, Nucl. Phys. B **220** [FS8], 415 (1983).

Received 28.02.14

П. Сарканич, Ю. Головач, Р. Кенна

ПРО ФАЗОВУ ДІАГРАМУ
ДВОВИМІРНОЇ МОДЕЛІ ІЗІНГА
ІЗ ДИПОЛЬНОЮ ВЗАЄМОДІЄЮ

Р е з ю м е

Через присутність у двовимірній фрустрованій моделі Ізінга конкуруючих феромагнітної взаємодії найближчих сусідів і далекосяжної антиферомагнітної дипольної взаємодії, цій моделі притаманна дуже складна фазова діаграма. Нещодавно з'явилися суперечливі дані щодо роду фазового переходу, який спостерігається в цій моделі, а саме переходу між смужковою $h = 1$ і тетрагональною фазами. Ми спробуємо відповісти на це питання опираючись на метод аналізу густини нулів статистичної суми в площині комплексної температури. Наші результати свідчать про наявність фазового переходу другого роду. Як кількісну характеристику фазового переходу ми використовуємо критичний показник питомої теплоємності α. Цей показник виявляється залежним не лише від вимірності простору, а і від співвідношення між параметрами взаємодії.